# Beware of Cocktails: Chain-Length Bidispersity Triggers Explosive Self-Assembly of Poly-L-Glutamic Acid β_2-Fibrils

Agnieszka Hernik-Magoń,[†] Wojciech Puławski,[†] Bartłomiej Fedorczyk,[†] Dagmara Tymecka,[†] Aleksandra Misicka,[†] Piotr Szymczak,[‡] and Wojciech Dzwolak*,[†]

[†]Department of Chemistry, Biological and Chemical Research Centre, and [‡]Institute of Theoretical Physics, Faculty of Physics, University of Warsaw, Warsaw, Poland

ABSTRACT: Chain-length polydispersity is among the least under-stood factors governing the fibrillation propensity of homopolypep-tides. For monodisperse poly-L-glutamic acid (PLGA), the tendency to form fibrils depends of the main-chain length. Long-chained PLGA, so-called $(Glu)_{200}$, fibrillates more readily than short $(Glu)_5$ fragments. Here we show that conversion of α-helical $(Glu)_{200}$ into amyloid-like β-fibrils is dramatically accelerated in the presence of intrinsically disordered $(Glu)_5$. While separately self-assembled fibrils of $(Glu)_{200}$ and $(Glu)_5$ reveal distinct morphological and infrared

characteristics, accelerated fibrillation in mixed $(Glu)_{200}$ and $(Glu)_5$ leads to aggregates similar to neat $(Glu)_{200}$ fibrils, even in excess of $(Glu)_5$. According to molecular dynamics simulations and circular dichroism measurements, local events of "misfolding transfer" from $(Glu)_5$ to $(Glu)_{200}$ may play a key role in the initial stages of conformational dynamics underlying the observed phenomenon. Our results highlight chain-length polydispersity as a potent, although so-far unrecognized factor profoundly affecting the fibrillation propensity of homopolypeptides.
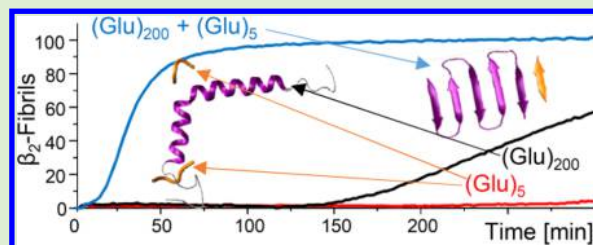
INTRODUCTION

The self-assembly of amyloid fibrils—linear β-sheet-rich protein aggregates linked to disorders such as Alzheimer's disease[1,2]—is a generic structural transition accessible to different proteins and peptides including homopolypeptides,[3] very short synthetic peptides,[4,5] polypeptides with randomized amino acid sequences,[6,7] and even non-α-poly amino acids.[8] Among several poly-α-amino acids forming such fibrils,[3,9,10] PLGA constitutes a very interest-ing case. Acidification of aqueous solutions of PLGA induces a rapid coil $\rightarrow$ helix transition.[11,12] The resulting α-helical con-formation is metastable at high PLGA concentrations and trans-forms spontaneously into insoluble β-aggregates (termed β_2) with the characteristic infrared trait: the amide I' band unusually red-shifted below 1600 cm^{-1},[13,14] which has been attributed to the networks of three-centered hydrogen bonds coupling side chain's carboxyl and main chain −NH groups as hydrogen donors to main chain >C=O groups as bifurcating acceptors.[14−19] Such aggregates reveal several properties characteristic for amyloid fibrils. We have shown recently that $(Glu)_n$ chains varying dramatically in length ($4 \leq n \leq 200$) appear to form β_2-amyloid fibrils according to a single structural theme as evidenced by the high degree of spectral and morphological similarities between thus obtained fibrils, as well as their ability to catalyze fibrillation of one another upon cross-seeding.[20]

Chemical uniformity of side groups in homopolypeptides allows one to explore fundamental effects of main-chain length on the amyloidogenic self-assembly,[21−23] which are otherwise eclipsed by specific contributions of amino acid sequences. Effects of chain-length polydispersity on fibrillation can also be addressed using homopolypeptide models but, surprisingly, have not been thoroughly studied so far.

Having observed that short and long PLGA chains form β_2-fibrils on different time-scales, we were initially interested in whether the less aggregation-prone pentapeptide $(Glu)_5$ could slow fibrillation of long-chained polymer $(Glu)_{200}$.[20] Unexpect-edly, the self-assembly of β_2-fibrils in mixed $(Glu)_5$ and $(Glu)_{200}$ samples proved to follow an explosive kinetic trajectory leading to a distinct type of aggregate and revealing a new aspect of dynamics of aggregating polypeptide chains.

EXPERIMENTAL SECTION

Samples. *(Glu)_{200}*. We use term "$(Glu)_{200}$" to refer to the particular commercial fraction of PLGA used in this study. $(Glu)_{200}$ (as sodium salt, cat. No. P4761, Lot # 096 K5103 V, molecular weight of 15−50 kDa) was from Sigma, USA. D$_2$O, DCl were purchased from ARMAR Chemicals, Switzerland. The $(Glu)_{200}$ lot used in this work is the same as in our previous studies and has been extensively characterized in terms of linearity and molecular weight.[17]

(Glu)_5. $(Glu)_5$ was obtained by means of solid phase peptide synthesis (SPPS) with the use of preloaded with Fmoc-Glu(OtBu)-Wang resin, as described in detail in our earlier work.[20] The crude product was analyzed using RP-HPLC, then purified and lyophilized. Purity of peptide samples was determined as 98 wt % by RP-HPLC and LC-IT-TOF mass spectrometry with an ESI ion source.

Preparation of β_2 Aggregates from $(Glu)_n$ Peptides. Unless otherwise noted in figure captions, the following protocol of prepara-tion of β_2-aggregates was employed. Peptides in the form of sodium

salts were dissolved in D_2O at 1 wt % concentration. Clear solutions were gradually acidified at room temperature with diluted DCl to pD 4.1 (uncorrected pH-meter readout) and subjected to 72-h-long quiescent incubation at 60 °C. Under these conditions, β_2-aggregates formed and precipitated over time. Insoluble aggregates were subsequently subjected to Fourier transform infrared (FT-IR)/atomic force microscopy (AFM) measurements. For kinetic experiments, freshly acidified peptide samples were swiftly transferred to thermostated CaF_2 cell. Depending on the case, seeds (i.e., fibrils preformed at 60 °C, as described above, and sonicated afterward) were added to the peptide solution at 1:33 seed:soluble peptide mass ratio (for seeding of 0.3 wt % samples of soluble peptides).

Static and Time-Lapse FT-IR Spectra. For acquisition of static FT-IR spectra, 256 interferograms of nominal resolution of 2 cm^{-1} were coadded. The spectra were acquired at 25 °C using a CaF_2 transmission cell and 0.05 mm Teflon spacer on Nicolet iS50 FT-IR spectrometer (Thermo, USA) equipped with a DTGS detector. During the measurements, spectrometer's sample chamber was continuously purged with dry air. Time-lapse FT-IR spectra were collected in a similar way; however, the number of interferograms coadded for a single spectrum was reduced to 16. During measurements, the temperature in the cell (40 °C) was controlled through a dedicated Peltier system. From each sample's spectrum, the corresponding buffer and water vapor spectra were subtracted. Baseline correction was performed with GRAMS software (Thermo). All further experimental details were the same as specified earlier.[20]

Atomic Force Microscopy (AFM). Collected samples of aggregates were initially diluted 100 times with slightly acidified H_2O (pH 4). A small droplet of 8 μL of fibril suspension was swiftly deposited onto freshly cleaved mica and left to dry for 24 h. AFM tapping-mode measurements were carried out using Nanoscope III atomic force microscope (Veeco, USA) and TAP300-Al sensors, res. frequency 300 kHz (BudgetSensors, Bulgaria).

Circular Dichroism (CD). Small samples of sodium salts of $(Glu)_{200}$ and $(Glu)_5$ were separately dissolved in portions of D_2O and acidified with diluted DCl to pD = 4.1 (uncorrected pH-meter readout). The concentration of peptide solutions for CD measurements was set at exactly 0.0025 wt %. The mixed $(Glu)_{200}$ + $(Glu)_5$ sample was obtained by swift mixing of two equal volumes of 0.0025 wt % stock solutions of both peptides. CD measurements in far-UV region were carried out immediately, as well as 30 and 60 min after sample preparation. Spectral data were collected at 40 °C (the temperature in the cell was maintained using a PC-controlled Peltier unit) by accumulation of five independent spectra on Jasco J-815 S spectropolarimeter (Jasco, Japan) equipped with high quality optical quartz cuvette with the path length of 10 mm. The CD difference spectra in Figure 5 were calculated by subtracting CD spectrum of the mixed sample from the sum of separately collected CD spectra of $(Glu)_{200}$ and $(Glu)_5$ according to the formula:

$$\Delta CD(\lambda, t) = \frac{1}{2}(CD_{(Glu)5}(\lambda, t) + CD_{(Glu)200}(\lambda, t))$$
$$- CD_{(Glu)5+(Glu)200}(\lambda, t)$$

where $CD(\lambda, t)$ refers to the CD signal at λ-wavelength of a given sample collected t minutes after the preparation/mixing (incubation at 40 °C). Because of different molecular masses of both peptides, we have chosen to express the measured CD signals in raw units ([mdegs]).

Molecular Dynamics (MD) simulations. Simulations were carried out using the Amber 14 package[24] and FF12SB force-field along with TIP3 water model. Specific conditions: time step of 2 fs under periodic boundary conditions with constant pressure and temperature was used. All nonbonding interactions were truncated with 9 Å cutoff, and for long-range electrostatics the PME algorithm was used. The SHAKE method constrained the length of the hydrogen bonds. The initial $(Glu)_{50}$ conformation was constructed as an ideal α-helix with 50 Glu residues (with side chains in the nonionized state) and $-NH_3^+$ and $-COOH$ groups for N-, and C-termini, respectively. Such ionization state corresponds to the charge distribution in PLGA dissolved at pH 4.1. The $(Glu)_5$ pentapeptide was initially an extended

chain. Subsequently, the $(Glu)_{50}$ helix was minimized in vacuum with $C\alpha$ atoms restrained, whereas pentapeptide was solvated in TIP3 water box and subjected to 10 ns dynamics, the representative structure from this procedure was used for MD afterward. The final starting system was created from $(Glu)_{50}$ helix and two $(Glu)_5$ pentapeptides (placed 5 and 7 Å away from the helix) and 24669 TIP3 water residues, resulting in the simulation box of 130 × 80 × 80 nm dimensions and 74957 atoms. Three chloride ions were added to compensate for the three positive charges at N-terminal $-NH_3^+$ groups and hence to provide overall electrical neutrality. The system was minimized for 2000 steps with all backbone atoms harmonically restrained to original positions (spring constant of 1.0 $kcal/mo/Å^2$), and subsequently subjected to gradual heating to 313.15 K during the first nanosecond, then equilibrated for the next 9 ns. Only $C\alpha$ atoms were harmonically restrained during this stage with a spring constant of 0.5 $kcal/mo/Å^2$. A simulation run was performed for the next 150 ns without any constraints. Molecular figures and visualizations were prepared using the VMD software.[25]

RESULTS AND DISCUSSION

Figure 1A shows typical time-lapse FT-IR spectra of an acidified aqueous sample of high molecular weight fraction of PLGA
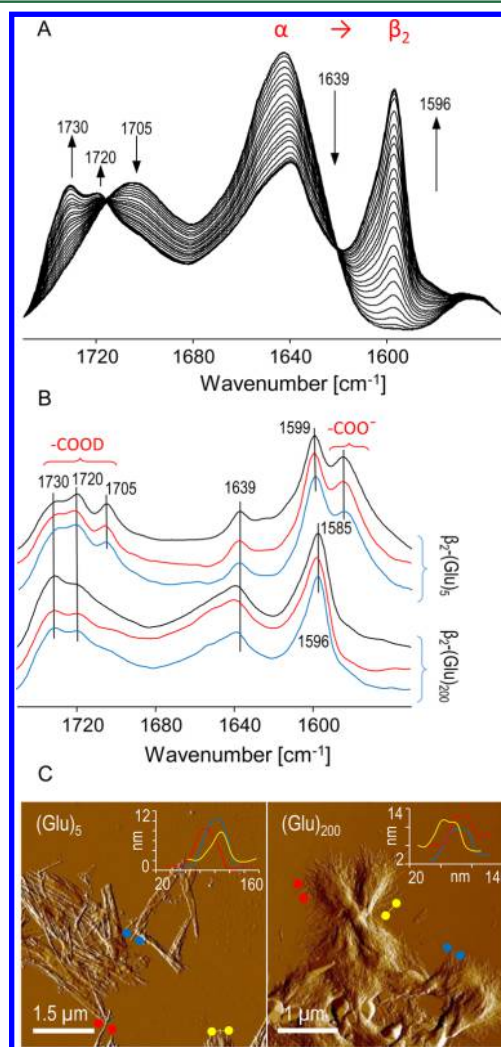

Figure 1. β_2-$(Glu)_n$ fibrils. (A) $\alpha \rightarrow \beta_2$ transition in PLGA (1 wt % of $(Glu)_{200}$ in D_2O, pD 4.1, 40 °C, 24 h) probed by time-lapse FT-IR spectroscopy (in the amide I' region). (B) Spectra of β_2-fibrils formed separately by $(Glu)_5$ and $(Glu)_{200}$ through the spontaneous aggregation (black lines), homologous seeding with preformed β_2-$(Glu)_n$ fibrils (red lines), and cross-seeding with alternative seeds (blue lines). (C) AFM images of β_2-$(Glu)_5$ and β_2-$(Glu)_{200}$ fibrils with cross sections of selected specimen.

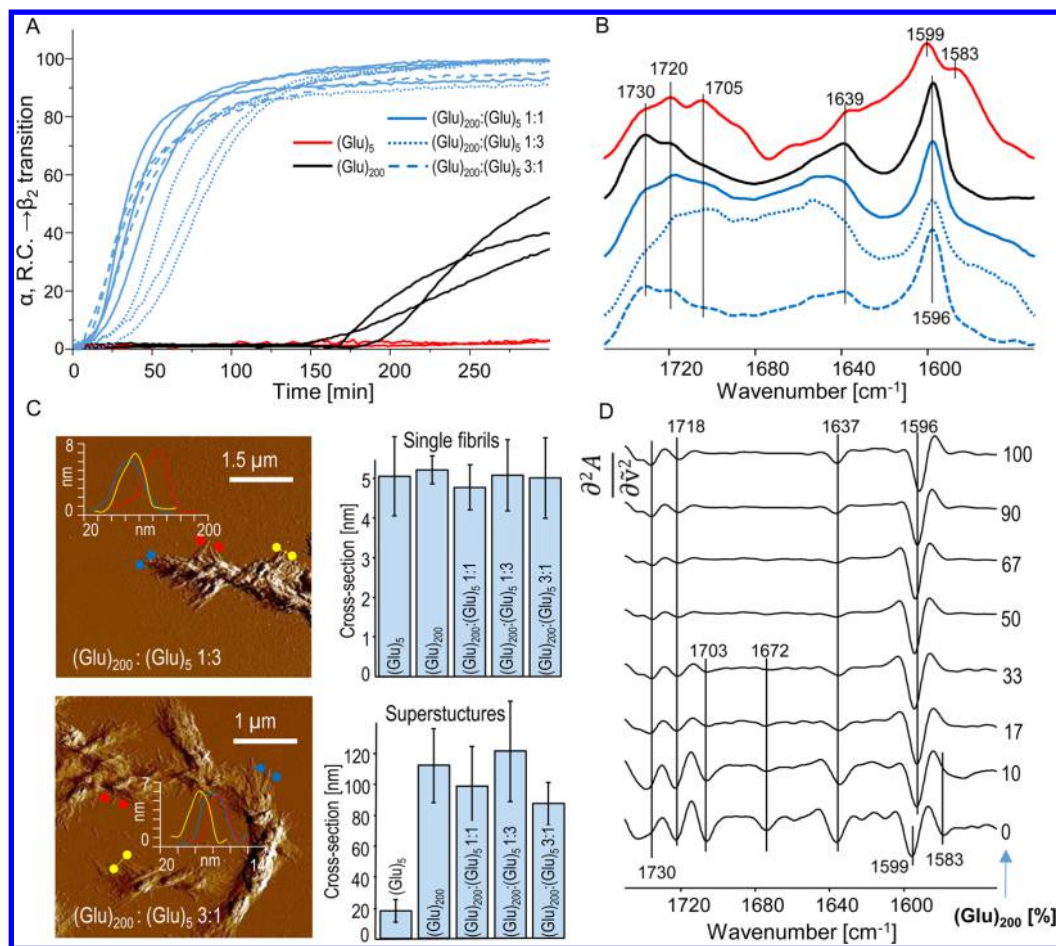**Figure 2.** Formation of β_2-fibrils in mixed solutions of $(Glu)_5$ and $(Glu)_{200}$ peptides. (A) Multiple kinetic trajectories of the α, R.C. $\rightarrow \beta_2$ transitions in $(Glu)_{200}$, $(Glu)_5$ and their mixtures at 40 °C according to spectral intensities of the β_2 component in the amide I′ band (total peptide concentration in D_2O, pD 4.1, was fixed at 0.3 wt %, different lines mark various $(Glu)_{200}$:$(Glu)_5$ ratios, as indicated). (B) Corresponding final infrared spectra of β_2-fibrils collected after 24 h. (C) AFM images of superstructural arrangements of β_2-fibrils formed in $(Glu)_{200}$ and $(Glu)_5$ mixed solutions at 1:3 and 3:1 mass ratios. Histograms show averaged AFM-collected diameters of single fibrils (top) and fibrillar superstructures (bottom). (D) 2nd derivative FT-IR spectra of β_2-fibrils formed in mixed solutions of $(Glu)_5$ and $(Glu)_{200}$ at different ratios, the mass percent of $(Glu)_{200}$ decreasing from top to bottom is indicated on the right.

(termed $(Glu)_{200}$) undergoing the conformational transition from the initially α-helical soluble form to insoluble β_2-fibrils. The extremely low frequency of the main amide I′ band component in β_2-$(Glu)_{200}$ spectra (ca. 1596 cm^{-1}) is a consequence of the presence of bifurcating hydrogen bonds involving hydrogen donors on both main and side chains.[14−19] The emergence of the 1596 cm^{-1} peak is synchronized with spectral changes in the region of side chains' − COOD groups (above 1700 cm^{-1}). Decreasing the chain-length of $(Glu)_n$ peptides decelerates the aggregation and affects infrared spectra of mature β_2-fibrils.[20] Hence, although the amyloidogenic self-assembly of $(Glu)_n$ chains appears to proceed according to a unified structural theme regardless of n, there are detectable spectral and morphological differences between β_2-$(Glu)_5$ and β_2-$(Glu)_{200}$ aggregates. Figure 1B presents FT-IR spectra of β_2-fibrils self-assembled from short $(Glu)_5$ (top three), and long $(Glu)_{200}$ chains (bottom three) according to different scenarios, namely, spontaneous *de novo* aggregation, homologous seeding, and cross-seeding. As the type of seed does not determine spectral features of daughter fibrils, no self-propagating polymorphism of fibrils is observed. For all $(Glu)_5$ aggregates, the main β_2-peak is shouldered by a new band at ca. 1585 cm^{-1} originating from antisymmetric stretches of ionized −COO$^-$ groups.[20,26]

We have argued recently that, despite the acidic environment, the formation of salt bridges with ionized N-terminal −NH$_3^+$ (−ND$_3^+$) groups within the compressed solvent-sequestered β_2-fibril matrix could keep C-terminal carboxyl groups in the ionized state.[20] Morphological distinction between $(Glu)_5$ and $(Glu)_{200}$ fibrils is straightforward according to amplitude atomic force microscopy (AFM) images shown in Figure 1C. Individual β_2-fibrils of either peptide share similar diameters of ca. 4−6 nm, but only β_2-$(Glu)_{200}$ amyloid tends to form well-defined twisted superstructures.

The key results of this study are shown in Figure 2. We have used time-lapse FT-IR spectroscopy to probe kinetics of the β_2-self-assembly for $(Glu)_5$, $(Glu)_{200}$ and their mixtures. As precursor concentration strongly affects fibrillation rates, the total peptide concentration used in the kinetic experiments was strictly controlled and fixed at 0.3 wt %. Figure 2A shows multiple kinetic trajectories plotted for the first 5 h according to transient intensities of β_2 infrared components. In nonmixed samples, $(Glu)_{200}$ undergoes the transition markedly faster than $(Glu)_5$. Interestingly, in mixed solutions, the aggregation becomes dramatically accelerated. In fact, the $\alpha \rightarrow \beta_2$ transition trajectories for 1:1 and 3:1 mixtures of $(Glu)_{200}$ and $(Glu)_5$ are as steep as in the case of typical seed-induced fibrillation,

although no seeds where added to initiate the fibrillation kinetics depicted in Figure 2A. For the three cases of heterogeneous aggregation examined, the transition is slowest in the case of samples with the highest $(Glu)_5$ concentration. In Figure 2B, FT-IR spectra collected after 24 h of incubation are shown. Strikingly, the 1585 cm^{-1} band characteristic for β_2-$(Glu)_5$ fibrils is not observed in the mixed samples, even when $(Glu)_5$ is the dominant ingredient. We also note that the exact position of the β_2 peak in all mixed aggregates (1596 cm^{-1}) corresponds to that of neat β_2-$(Glu)_{200}$ fibrils, rather than of β_2-$(Glu)_5$ fibrils (1599 cm^{-1}). In the region of −COOD vibrations, the 1705 cm^{-1} band characteristic for $(Glu)_5$ appears to be relatively well preserved in the spectra of mixed aggregates.

In accordance with the data shown in Figure 2B, the morphology of mixed aggregates is clearly reminiscent of neat β_2-$(Glu)_{200}$ fibrils (vide AFM images in Figure 2C). The images of mixed aggregates, irrespective of $(Glu)_{200}$:$(Glu)_5$ ratio reveal a strong tendency of individual fibrils to associate laterally and form higher-order structures that are typical for β_2-$(Glu)_{200}$. The apparent scarcity of β_2-$(Glu)_5$-like singly dispersed fibrils suggests that the pentapeptide, instead of self-assembling according to its own amyloidogenic pathway, merged with $(Glu)_{200}$ chains to follow the PLGA's fibrillation pattern. The ensuing analysis of thickness of individual fibrils and their superstructural arrangements (histograms in Figure 2C) further supports the idea that the morphological "phenotype" of β_2-$(Glu)_{200}$ amyloid prevails in the mixed aggregate samples. In order to assess how dominating is the parent $(Glu)_{200}$ morphological motive, we have carried out a titration experiment in which aggregates formed in samples representing a wider range of $(Glu)_{200}$: $(Glu)_5$ ratios were examined using second derivative infrared spectroscopy. According to Figure 2D the increasing $(Glu)_5$ mass concentration has practically no visible impact on the spectra of mixed aggregates until it reaches the level of 70−80%.

The picture emerging from the so-far presented data is that of $(Glu)_{200}$ helices recruiting shorter $(Glu)_5$ chains (which, due to the insufficient length, must remain unstructured in solution) to follow the self-assembly pattern normally accessible only to long-chained PLGA. Given the fact that α-helical $(Glu)_{200}$ is metastable under these conditions in respect to β_2-fibrils, one could wonder whether $(Glu)_5$ acts only as catalyst of transition of $(Glu)_{200}$ while itself remaining in solution throughout the fibrillation process. For one, this seems implausible in light of the very effective cross-seeding between β_2-$(Glu)_{200}$ and β_2-$(Glu)_5$ fibrils,[20] i.e., stochastic formation of first β_2-$(Glu)_{200}$ or β_2-$(Glu)_5$ nuclei would trigger fast fibrillation of all the $(Glu)_n$ chains remaining in solution. Such scenario is unlikely, however, considering the absence of conformational imprinting between β_2-$(Glu)_{200}$ and β_2-$(Glu)_5$ upon cross-seeding;[20] infrared spectra of mixed aggregates induced by seeds are expected to resemble the weighted arithmetic mean of neat β_2-$(Glu)_{200}$ and β_2-$(Glu)_5$ spectra, which is clearly not the case here (vide spectra in Figures 2B and 1B). In other words, the mixed aggregates of short and long $(Glu)_n$ chains form through *conucleation* of both chains. It should also be stressed that the data presented in Figure 2B−D correspond not to the precipitating fractions, but to the whole samples. This is specifically supported by the auxiliary data in Figure 3. In order to check whether there is any significant fraction of either peptide unconverted into mixed β_2-fibrils and remaining in solution after the 24 h of incubations, an additional experiment was conducted in which FT-IR spectra
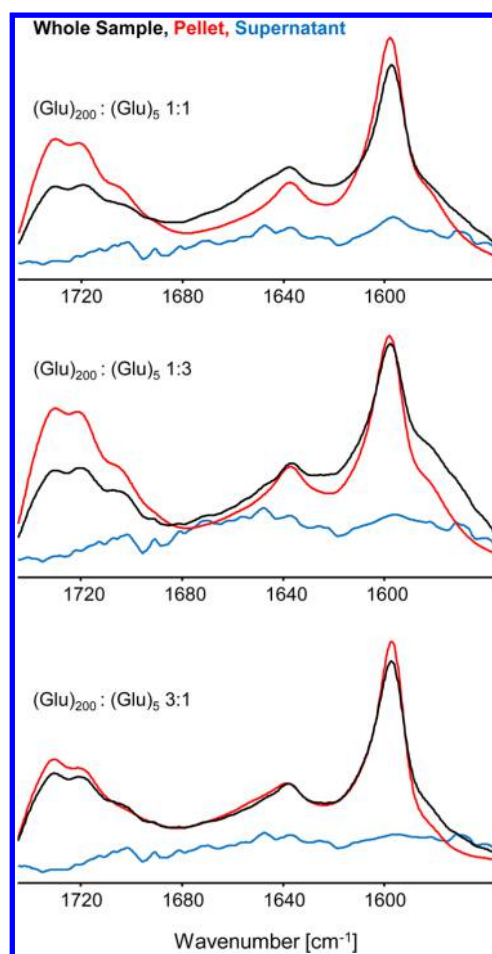

Figure 3. FT-IR spectra of β_2-fibrils formed in mixed solutions of $(Glu)_5$ and $(Glu)_{200}$ peptides (conditions as specified in Figure 2). Black lines correspond to the whole samples, red lines mark spectra of centrifuge-separated pellets, and blue lines correspond to the spectra of the clear remaining supernatants.

were measured for: [i] whole mixed samples prepared through the 24 h-long incubation (0.3 wt % total, D$_2$O, pD 4.1, 40 °C), [ii] centrifuged precipitates of β_2-fibrils (5 min at 13.400 rpm), and [iii] remaining clear supernatants. According to Figure 3, in the mixed samples, both $(Glu)_{200}$ and $(Glu)_5$ quantitatively coprecipitate, leaving negligible concentration of residual soluble peptide.

We have employed all-atom MD simulations to gain additional insights into early stages of coaggregation of $(Glu)_5$ and $(Glu)_{200}$. As long time-scales of diffusion-dependent conformational transitions accompanying PLGA aggregation would be very demanding in terms of computational power, instead we have focused on early stages (150 ns) of the self-assembly process by simulating the conformation of helical polyglutamate chain in the presence of two $(Glu)_5$ peptides. Due to computational costs, the excessively long $(Glu)_{200}$ was replaced with shorter $(Glu)_{50}$ fragment. The 50-residue-long peptide is sufficiently long to adopt (just like $(Glu)_{200}$) α-helical conformation in acidified aqueous environment.[27] The red RMSD trajectories in Figure 4A depict structural changes taking place in the α-helical backbone of $(Glu)_{50}$ upon interactions with the two added $(Glu)_5$ fragments. The increased RMSD sets in very early and further increases after the first 100 ns for three out of four simulated trajectories. Meanwhile, control trajectories for the $(Glu)_{50}$ helix simulated in the absence of
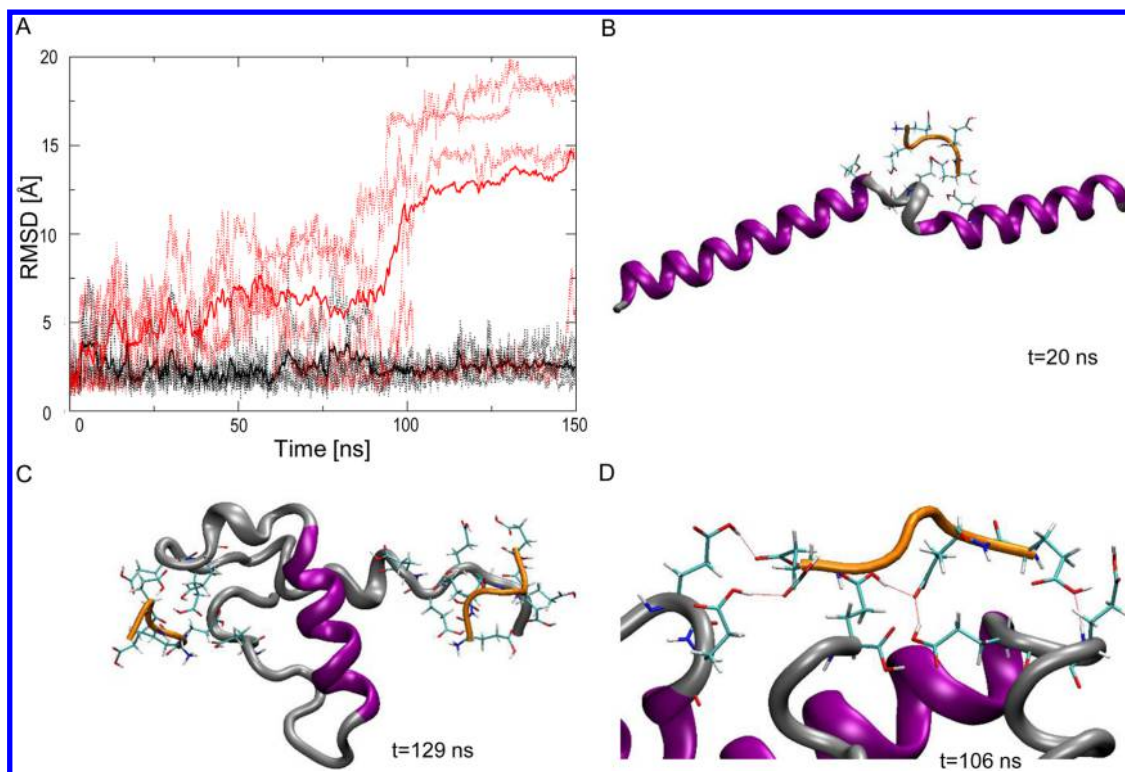
Figure 4. (A) MD trajectories depict root-mean-square deviation (RMSD) of C-α atoms of helical $(Glu)_{50}$ in the presence of two unstructured $(Glu)_5$ peptides (red dotted lines), and, in control simulations, of $(Glu)_{50}$ alone (black dotted lines). The superimposed thick red and black lines represent the averages of four independent trajectories obtained for either case. (B–D) Snapshots of different stages of interactions between $(Glu)_{50}$ and $(Glu)_5$ fragments leading to gradual accumulation of folding defects (local unfolding/bending events) within the $(Glu)_{50}$ helix. Backbone with the dihedral angles Φ and Ψ within the limits typical for the α-helical structure are marked in violet. In the (D) image, disruptive hydrogen bonds between $(Glu)_5$ side-chains and $(Glu)_{50}$ backbone are highlighted.

$(Glu)_5$ fragments remain flat (black trajectories), indicating thereby that the helix itself is relatively stable under these conditions. The snapshots shown in Figure 4 (panels B and C) represent some of the typical distortions of the helix upon binding to unstructured $(Glu)_5$ fragments observed at different stages of the simulation. Contact interactions between $(Glu)_5$ and $(Glu)_{50}$ were often found to take place both in the interior (B) and at the termini (C) of the helix, in each case leading swiftly to local structural defects of the latter. Such *misfolding-transfer* events were typically initiated by the formation of single hydrogen bonds between $(Glu)_5$ side chains and side chains of the helical peptide (Figure 4D) and tended to progress into local unfolding of the helix, followed by formation of additional hydrogen bonds between $(Glu)_5$ side chains and $(Glu)_{50}$ backbone and larger changes in the helix geometry. While no β-sheet formation was observed on the time-scales accessible to our computational resources, local unfolding is a recognized condition for formation of aggregation-competent states in proteins.[1,2] It is also known that α-helical poly-L-lysine chains with high content of locally disordered turns and loops reveal an increased tendency to form an intermolecular β-sheet.[21]

The very pronounced differences in the helical stability of $(Glu)_{50}$ in the presence and absence of $(Glu)_5$ emerging from the MD data reported in Figure 4 prompted our interest as to whether there is any experimentally detectable decrease in helicity of long-chained PLGA when $(Glu)_5$ is added. Certainly, such measurements would need to be carried out in a regime disfavoring aggregation and formation of fibrils, for example, at high dilution. To this effect, we have employed far-UV circular dichroism (CD) spectroscopy, which is not only a sensitive
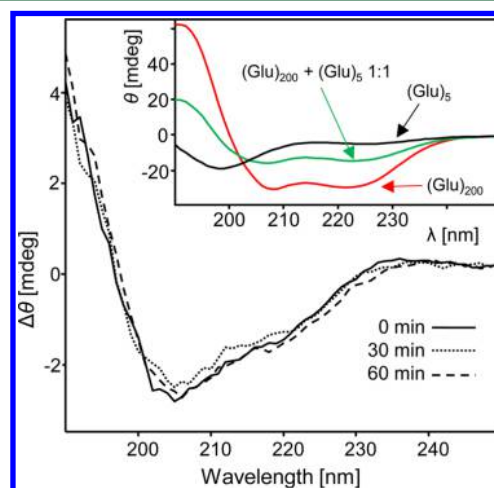

Figure 5. Differential CD spectra of diluted acidified $(Glu)_5$ and $(Glu)_{200}$ peptides and their approximately equimolar (in terms of Glu residues) mixture collected at 40 °C immediately after mixing, as well as after 30 and 60 min later. Inset shows original far UV-CD spectra of the three different samples.

probe of helical and disordered conformations, but also adapts well to the high dilution requirement. In Figure 5, difference far-UV CD spectra of separately dissolved and subsequently mixed $(Glu)_5$ and $(Glu)_{200}$ samples collected immediately after preparation, as well as 30 and 60 min later are shown. With the double minima, one at approximately 205 nm and another poorly resolved at 220 nm, the shape of the spectra corresponds

to distorted helical structures. More importantly, the negative sign of the spectra implies an effective net decrease in helicity of approximately 15% upon mixing of the two peptides. The spectra remain stable over the period of 1 h proving a significant deceleration of the $\alpha \rightarrow \beta_2$ transition in highly diluted $(Glu)_5 + (Glu)_{200}$ solution. The observed decrease in the helical CD signal appears to give strong support to the $(Glu)_5 \rightarrow (Glu)_{200}$ misfolding-transfer scenario that have emerged from the MD simulations.

In this study, we have shown that interactions in solution of long and short chains of a single homopolypeptide type (with moderate and low amyloidogenic propensities, respectively) lead to dramatic acceleration of conformational events on its fibrillation pathway. To our best knowledge, this observation has no similar precedence in the field of amyloid research. The reported counterintuitive behavior of mixed $(Glu)_n$ chains contrasts with our earlier results on coaggregation of short and long chains of poly(L-lysine), which form intermolecular β-sheet structure at a temperature intermediate with respect to nonmixed low- and high-molecular weight samples.[21] Our here presented results also imply that misfolding transfer between transient polypeptide conformations may play an important role in the emergence of the enhanced propensity to aggregate of bidisperse $(Glu)_n$ samples. The magnitude of the observed acceleration of fibrillation in mixed $(Glu)_{200}/(Glu)_5$ samples, and the fact that—in the absence of seeding memory effects (see Figure 1B)—properties of mixed aggregates are disproportionally dominated by the single ingredient $(Glu)_{200}$, are two puzzling aspects of the herein presented data. There are recently published studies on enhanced thermodynamic stability of self-assembled structures from polydisperse polymers[23] and on the emergence of distinct amyloid structure upon coaggregation of two amyloidogenic proteins.[28] The results presented in this study indicate that polymorphism of amyloid aggregates is an aspect of structural complexity accessible already to "sequenceless proteins" such as PLGA, and highlight chain-length polydispersity of polypeptides as a possible trigger factor in amyloidogenic self-assembly. The most clinically important problem of homopolypeptide amyloidogenesis concerns disorders (e.g., Huntington disease) linked to aggregation of proteins containing long polyglutamine sequences.[29] The correspondence between the length of monodisperse polyglutamine sections and severity of the illness is known. It remains to be seen whether transient increases in polydispersity of polyglutamine chains (e.g., caused by a local activity of proteases) could play a role in initiation of the amyloidogenic self-assembly in vivo. Certainly, further efforts are urgently needed in order to assess how common among amyloidogenic homopolypeptides is the phenomenon described here.

CONCLUSIONS

In summary, we have shown that the amyloidogenic self-assembly of helical long-chained PLGA is unexpectedly accelerated in the presence of short pentapeptidic PLGA fragments, which themselves are refractory to aggregation. The results of AFM- and FT-IR-based characterization of the mixed PLGA aggregates suggests that conucleation of both peptides plays a key role in the overall kinetics of fibrillation. According to the MD simulations and CD measurements, misfolding-transfer from the inherently unstructured peptapeptide to the helical long-chained PLGA may contribute to the latter becoming a more fluctuating and therefore aggregation-prone intermediate state. Our results point to chain-length polydispersity as yet another factor strongly influencing the amyloidogenesis of polypeptides.

AUTHOR INFORMATION

Corresponding Author

*E-mail: wdzwolak@chem.uw.edu.pl.

Notes

The authors declare no competing financial interest.

REFERENCES

(1) Chiti, F.; Dobson, C. M. Protein Misfolding, Functional Amyloid, and Human Disease. *Annu. Rev. Biochem.* **2006**, *75*, 333–366.

(2) Uversky, V. N.; Fink, A. L. Conformational Constraints for Amyloid Fibrillation: The Importance of Being Unfolded. *Biochim. Biophys. Acta, Proteins Proteomics* **2004**, *1698*, 131–153.

(3) Fändrich, M.; Dobson, C. M. The Behaviour of Polyamino Acids Reveals an Inverse Side Chain Effect in Amyloid Structure Formation. *EMBO J.* **2002**, *21*, 5682–5690.

(4) Reches, M.; Gazit, E. Casting metal nanowires within discrete self-assembled peptide nanotubes. *Science* **2003**, *300*, 625–627.

(5) de Groot, N. S.; Parella, T.; Aviles, F. X.; Vendrell, J.; Ventura, S. Ile-Phe dipeptide self-assembly: clues to amyloid formation. *Biophys. J.* **2007**, *92*, 1732–1741.

(6) Colaco, M.; Park, J.; Blanch, H. The Kinetics of Aggregation of Poly-glutamic Acid Based Polypeptides. *Biophys. Chem.* **2008**, *136* (2), 74–86.

(7) Lai, J.; Fu, W.; Zhu, L.; Guo, R.; Liang, D.; Li, Z.; Huang, Y. Fibril Aggregates Formed by a Glatiramer-Mimicking Random Copolymer of Amino Acids. *Langmuir* **2014**, *30* (24), 7221–7226.

(8) Lai, J.; Zheng, C.; Liang, D.; Huang, Y. Amyloid-like Fibrils Formed by ε-Poly-L-lysine. *Biomacromolecules* **2013**, *14* (12), 4515–4519.

(9) Dzwolak, W.; Ravindra, R.; Nicolini, C.; Jansen, R.; Winter, R. The diastereomeric assembly of polylysine is the low-volume pathway for preferential formation of β-sheet aggregates. *J. Am. Chem. Soc.* **2004**, *126*, 3762–3768.

(10) Smirnovas, V.; Winter, R.; Funck, T.; Dzwolak, W. Thermodynamic properties underlying the α-helix-to-β-sheet transition, aggregation, and amyloidogenesis of polylysine as probed by calorimetry, densimetry, and ultrasound velocimetry. *J. Phys. Chem. B* **2005**, *109*, 19043–19045.

(11) Yan, J. F.; Vanderkooi, G.; Scheraga, H. A. Conformational Analysis of Macromolecules. V. Helical Structures of Poly-L-aspartic Acid and Poly-L-glutamic Acid, and Related Compounds. *J. Chem. Phys.* **1968**, *49*, 2713–2726.

(12) Appel, P.; Yang, J. T. Helix-Coil Transition of Poly-L-glutamic Acid and Poly-L-lysine in D₂O. *Biochemistry* **1965**, *4*, 1244–1249.

(13) Itoh, K.; Foxman, B. M.; Fasman, G. D. The Two β Forms of Poly (L-glutamic acid). *Biopolymers* **1976**, *15*, 419–455.

(14) Fulara, A.; Dzwolak, W. Bifurcated Hydrogen Bonds Stabilize Fibrils of Poly (L-glutamic) Acid. *J. Phys. Chem. B* **2010**, *114*, 8278–8283.

(15) Fulara, A.; Lakhani, A.; Wójcik, S.; Nieznańska, H.; Keiderling, T. A.; Dzwolak, W. Spiral Superstructures of Amyloid-like Fibrils of Polyglutamic Acid: An Infrared Absorption and Vibrational Circular Dichroism Study. *J. Phys. Chem. B* **2011**, *115*, 11010–11016.

(16) Yamaoki, Y.; Imamura, H.; Fulara, A.; Wójcik, S.; Bożycki, Ł.; Kato, M.; Keiderling, T. A.; Dzwolak, W. An FT-IR Study on Packing Defects in Mixed β-Aggregates of Poly (L-glutamic acid) and Poly (D-

glutamic acid): A High-Pressure Rescue from a Kinetic Trap. *J. Phys. Chem. B* **2012**, *116*, 5172−5178.

(17) Fulara, A.; Hernik, A.; Nieznańska, H.; Dzwolak, W. Covalent Defects Restrict Supramolecular Self-Assembly of Homopolypeptides: Case Study of *β*2-Fibrils of Poly-L-Glutamic Acid. *PLoS One* **2014**, *9*, e105660.

(18) Chi, H.; Welch, W. R.; Kubelka, J.; Keiderling, T. A. Insight into the Packing Pattern of *β*2 Fibrils: A Model Study of Glutamic Acid Rich Oligomers with 13C Isotopic Edited Vibrational Spectroscopy. *Biomacromolecules* **2013**, *14*, 3880−3891.

(19) Kessler, J.; Keiderling, T. A.; Bour, P. Arrangement of Fibril Side Chains Studied by Molecular Dynamics and Simulated Infrared and Vibrational Circular Dichroism Spectra. *J. Phys. Chem. B* **2014**, *118*, 6937−6945.

(20) Hernik, A.; Puławski, W.; Fedorczyk, B.; Tymecka, D.; Misicka, A.; Filipek, S.; Dzwolak, W. Amyloidogenic Properties of Short *α*-L-glutamic Acid Oligomers. *Langmuir* **2015**, *31*, 10500−10507.

(21) Dzwolak, W.; Muraki, T.; Kato, M.; Taniguchi, Y. Chain-length Dependence of *α*-helix to *β*-sheet Transition in Polylysine: Model of Protein Aggregation Studied by Temperature-Tuned FTIR Spectroscopy. *Biopolymers* **2004**, *73* (4), 463−469.

(22) Ricchiuto, P.; Brukhno, A. V.; Paci, E.; Auer, S. Communication: Conformation State Diagram of Polypeptides: A Chain Length Induced *α*-*β* Transition. *J. Chem. Phys.* **2011**, *135* (6), 061101.

(23) Widin, J. M.; Schmitt, A. K.; Schmitt, A. L.; Im, K.; Mahanthappa, M. K. Unexpected Consequences of Block Polydispersity on the Self-Assembly of ABA Triblock Copolymers. *J. Am. Chem. Soc.* **2012**, *134* (8), 3834−3844.

(24) Case, D. A.; Babin, V.; Berryman, J. T.; Betz, R. M.; Cai, Q.; Cerutti, D. S.; Cheatham, T. E.; Darden, D. A., III; Duke, R. E.; Gohlke, H.; Goetz, A. W.; Gusarov, S.; Homeyer, N.; Janowski, P.; Kaus, J.; Kolossváry, I.; Kovalenko, A.; Lee, T. S.; LeGrand, S.; Luchko, T.; Luo, R.; Madej, B.; Merz, K. M.; Paesani, F.; Roe, D. R.; Roitberg, A.; Sagui, C.; Salomon-Ferrer, R.; Seabra, G.; Simmerling, C. L.; Smith, W.; Swails, J.; Walker, R. C.; Wang, J.; Wolf, R. M.; Wu, X.; Kollman, P. A. *AMBER 14*; University of California: San Francisco, CA, 2014.

(25) Humphrey, W.; Dalke, A.; Schulten, K. VMD: Visual Molecular Dynamics. *J. Mol. Graphics* **1996**, *14*, 33−38.

(26) Barth, A. The Infrared Absorption of Amino Acid Side Chains. *Prog. Biophys. Mol. Biol.* **2000**, *74*, 141−173.

(27) Rinaudo, M.; Domard, A. Circular Dichroism Studies on alpha-L-glutamic Acid Oligomers in Solution. *J. Am. Chem. Soc.* **1976**, *98*, 6360−6364.

(28) Sarell, C. J.; Woods, L. A.; Su, Y.; Debelouchina, G. T.; Ashcroft, A. E.; Griffin, R. G.; Stockley, P. G.; Radford, S. E. Expanding the Repertoire of Amyloid Polymorphs by Co-Polymerization of Related Protein Precursors. *J. Biol. Chem.* **2013**, *288* (10), 7327−7337.

(29) Wetzel, R. Physical Chemistry of Polyglutamine: Intriguing Tales of a Monotonous Sequence. *J. Mol. Biol.* **2012**, *421* (4), 466−490.